

## **"Laminar flow through fuel cell stacks"**

Anas Ahmed Elamin Ahmed

### **Synopsis**

This study aims to do a numerical simulation using OpenFOAM v2012 of laminar flow through single sharp and curved bends channels of typical fuel cell configurations, for steady laminar flows, a systematic numerical study conducted to understand the flow structure and related phenomena in laminar flow through 90° bend over a range of curvature ratios and aspect ratios. The geometry and mesh were defined using the blockMesh utility. A steady-state, SIMPLE algorithm-based simpleFoam solver was used in the simulation. The analysis was executed by S. Jayanti, S. Maharudrayya, A.P. Deshpande [1] using the CFD Center, IIT-Madras, India.

### **References:**

[1] "Pressure losses in laminar flow through serpentine channels in fuel cell stacks", S. Jayanti, S. Maharudrayya, A.P. Deshpande, Department of Chemical Engineering, IIT Madras, India, June 2004.

## 1 Introduction

In the reference paper [1], the CFD-based simulations have been conducted for 90° bend with different curvature ratios (C) and different aspect ratios (A). The effect of successive bends for various Reynolds numbers under a laminar flow regime has been examined. The simulation shows that there is a significant effect of Re on the bend loss, which is also influenced by the curvature ratio and the aspect ratio as well as the presence of an upstream bend. The paper reference [2] finds the flow separation characteristics under a high Reynolds number in pipe bends. Single-phase turbulent flow through pipe bends is investigated using the k-ε turbulence model. The nominal fluid properties of gas corresponded to those of air at atmospheric conditions (kinematic viscosity of air at 15° C is 1.48e-5 m<sup>2</sup>/s and density is 1.22 kg/m<sup>3</sup>).

## 2 Governing Equations and Boundary Conditions

To reproduce results generated by S. Jayanti [1], OpenFOAM foam v2012 software was used. The governing equations, assuming incompressibility are:

### 2.1 Mass balance equation:

$$\frac{\partial U_i}{\partial x_i} = 0$$

### 2.2 Momentum balance equation:

$$\frac{\partial (U_i U_j)}{\partial x_j} = -\frac{1}{\rho} \frac{\partial P}{\partial x_i} + \frac{\partial}{\partial x_i} \left( \nu \frac{\partial U_j}{\partial x_j} \right)$$

Here,  $U_i$  is the component of velocity in the i-direction;  $P$  is the static pressure,  $\rho$  and  $\nu$  are the fluid density and kinematics viscosity, respectively.

### 2.3 Boundary conditions:

The boundary conditions imposed were (also see Table 2.1):

1. Normal velocity specified as the mean flow velocity at the upstream ‘inlet’
2. Fully developed flow condition specified at the downstream ‘outlet’.
3. no-slip condition on the sidewalls;
4. Symmetry condition (zero normal gradients) specified on the symmetry plane.

Table 2.1: Boundary conditions

Field Variable	Inlet	Wall	Outlet
Velocity	Fixed – Uniform Velocity Profile	No-Slip	Zero Gradient
Pressure	Zero Gradient	Zero Gradient	Fixed – Zero Value

### 3 Simulation Procedure

#### 3.1 Geometry and Mesh

The geometries were generated by using multi-block mesh (3 blocks) and assumed the length of blocks is 3 mm, the channels with six aspect ratios are generated, shown in Figure 1. The curved channel with a constant hydraulic diameter, which is 10.06 mm,  $D_h = 4wh/2(w + h)$ , where  $w$  and  $h$  are the width and depth of the channel respectively, with three Curvature ratios,  $C = R_c/D_h$ , and aspect ratio  $A = 2.77$  are shown in Figure 2. Only one-half of the duct cross-section will be simulated by taking advantage of the symmetry plane.

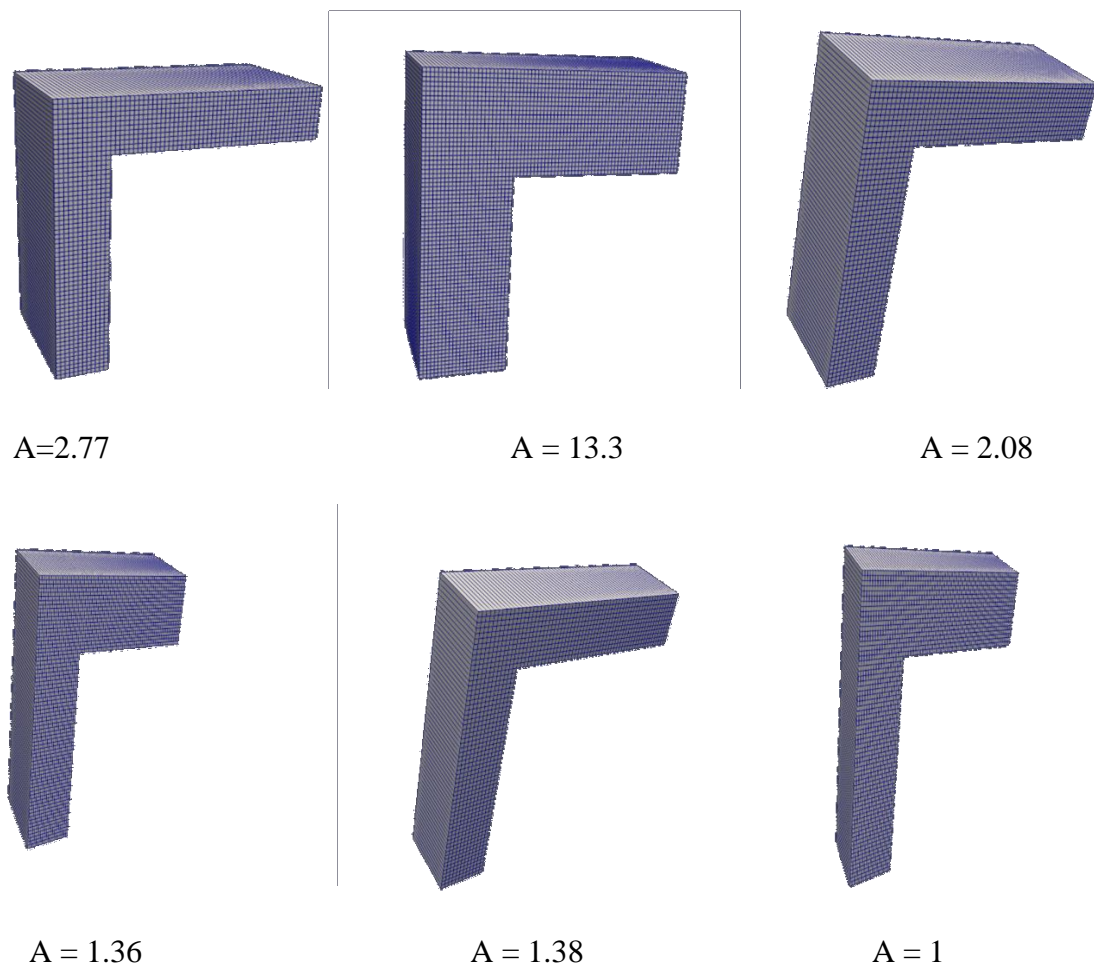


Figure 1: The geometry with different aspect ratios.

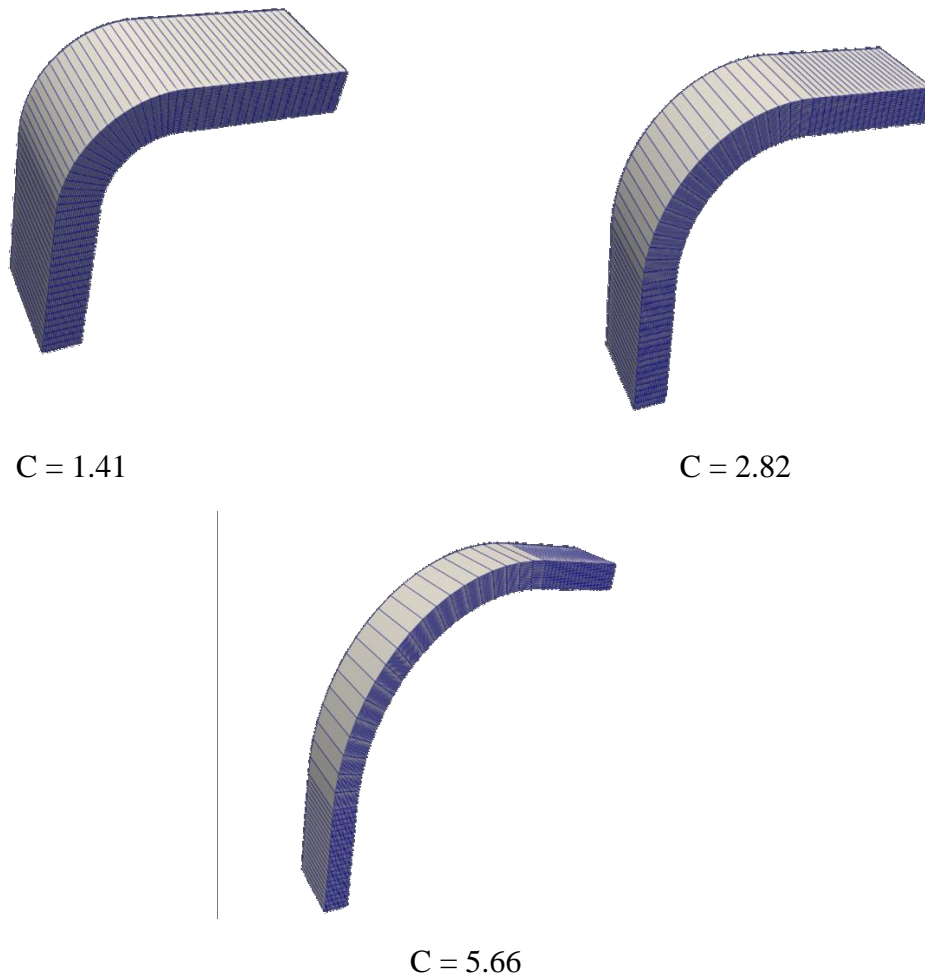


Figure 2: The geometry with different curvature ratios.

### 3.2 Solver

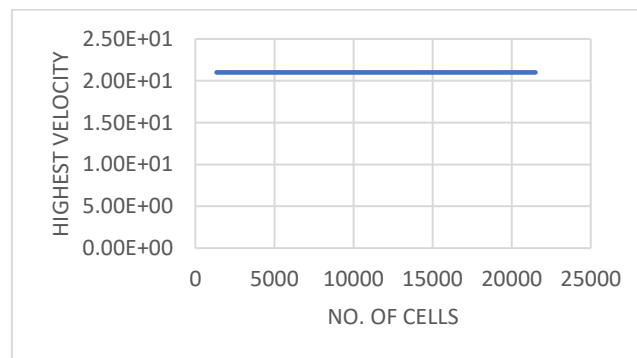
A steady-state for incompressible, turbulent flow-based simpleFoam solver is used to run governing equations in the discretized domain. The simpleFoam solver uses the SIMPLE (Semi-Implicit Method for Pressure Linked Equations) algorithm to evaluate N.S equations. The solver follows a segregated solution strategy. This means that the equations for each variable characterizing the system (the velocity  $u$ , the pressure  $p$ , and the variables characterizing turbulence) are solved sequentially, by removing the turbulence and making it laminar, it becomes suitable for this case. For the convergence, a simulation was used with 1000 maximum iterations for simulation of the flow-through channels and used 1000 for heat transfer simulation.

## 4 Grid Independence Study and Validation

### 4.1 Grid independence test

The grid independence test was done to find the difference in the numerical results, the sharp channel with an aspect ratio of 2.77 and  $Re = 700$  was tested in different mesh sizes, the number of cells for each block (3 blocks) increased double for the test 1, 2 and 3, the total number of cells of geometry was 1344, 5376, and 21504 for three tests respectively, and the three results show that there is no difference between tests which are done, see Figure 3.

(a)



(b)

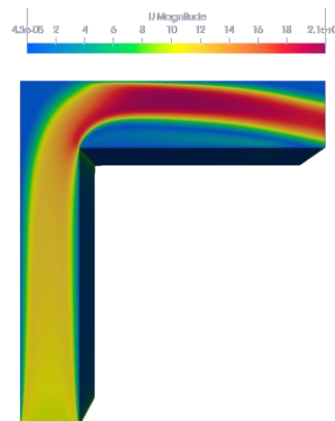
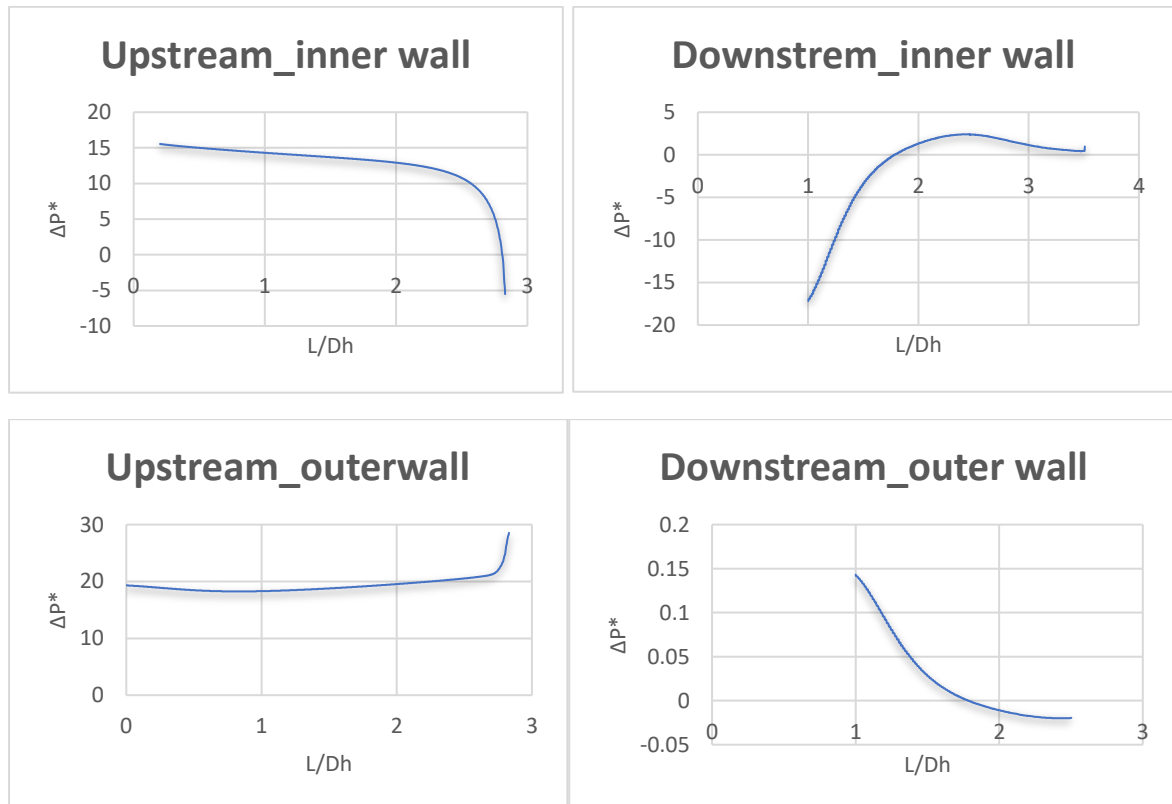


Figure 3(a): Mesh independence test plot. (b): The results of the simulation for the sharp channel with  $A = 2.77$  &  $Re = 700$  with the different mesh sizes.

## 4.2 Validation

Validation of the methodology is provided in Figure 4(a), where the variation of the dimensionless static pressure drop (pressure drop/kinetic head) along the inner and the outer walls were plotted and it follows the same brand of the plot shown in Figure 4(b) which is presented in the reference paper [1].

(a)



(b)

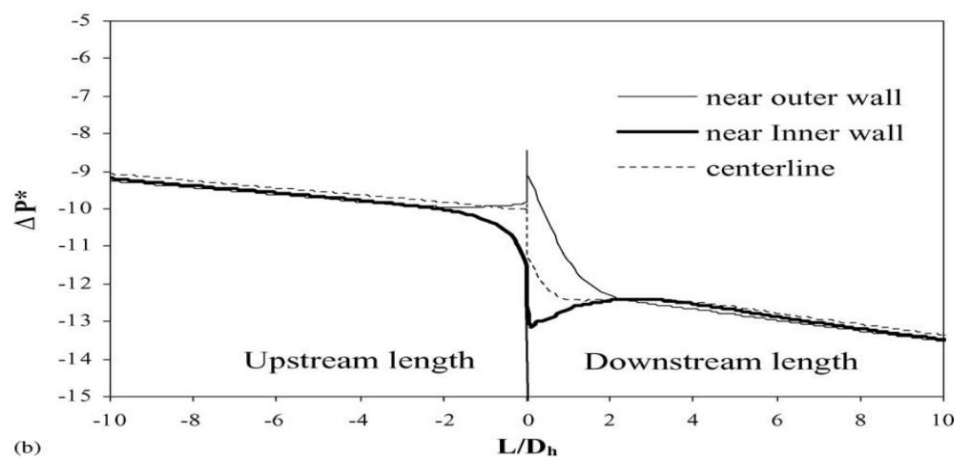


Figure 4. (a): Variation of dimensionless static pressure along inner and outer walls in symmetry plane for a sharp bend. (b): Variation of dimensionless static pressure along the center-line of the duct and inner and outer walls in symmetry plane for the sharp bend [1].

## 5 Results and Discussions

For the comparison of the results, pressure drop was plotted, to show the effect of losses with skin friction, bends, and Reynolds number, the streamlines were plotted for comparison of the velocity. The results were compared with the experimental data or the reference paper [1].

Figures 5, 6, and 7(a) compare pressure drops and velocity effects over different geometries and Reynolds numbers used in the simulations. The results show that a significant pressure decrease occurs within the bend, but it varies depending on the aspect and curvature ratios. Several configurations were studied using this methodology.

A typical variation of the velocity (plotted in terms of streamlines of the velocity) in the symmetry plane in the region of the bend (Re of 700, sharp bend with aspect ratio 2.77) is shown in Figure 5(a). There is significant distortion of the velocity field as the flow goes through the bend and a large recirculation bubble downstream of the bend can be seen.

(a)



(b)

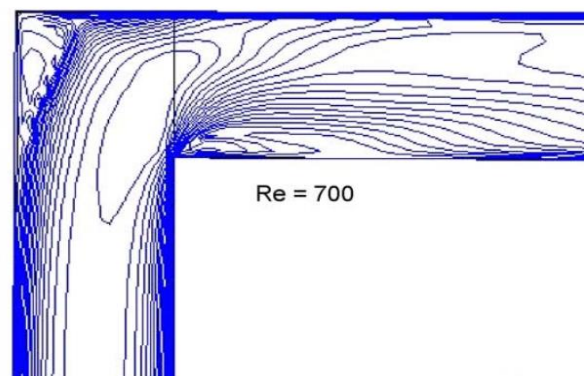
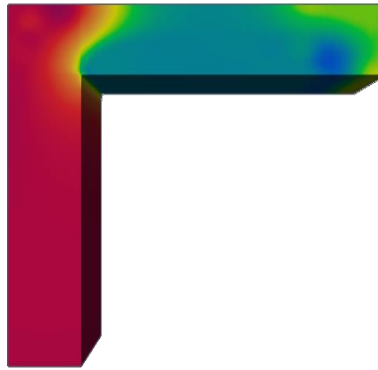


Figure 5. (a): Velocity streamlines plot in symmetry plane for sharp bend at Reynolds number of 700. (b): Velocity contour plot in symmetry plane for sharp bend at Reynolds number of 700 [1].

(a)



(b)

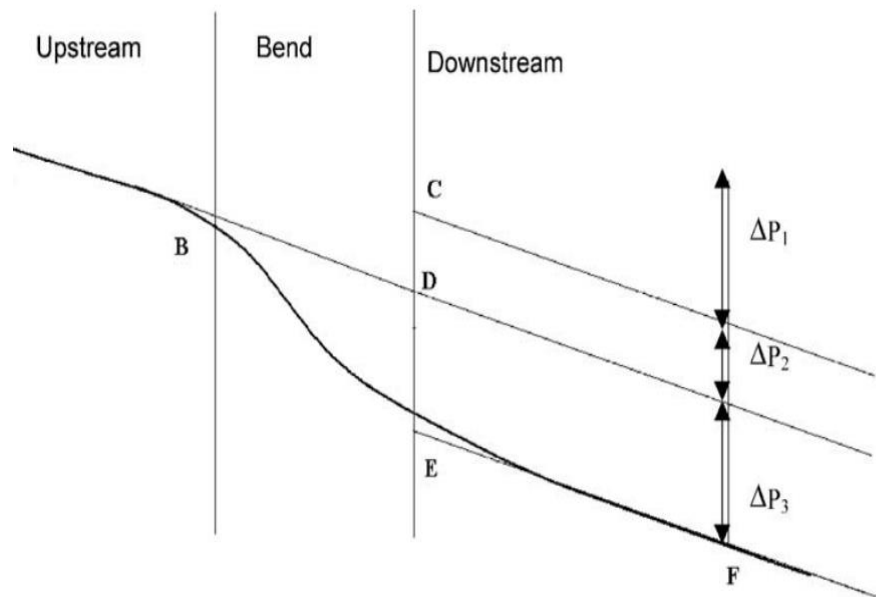
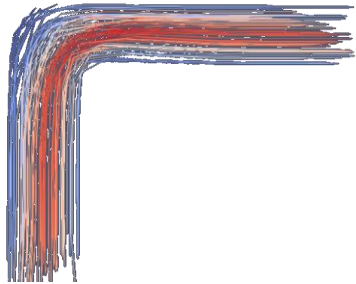


Figure 6. (a): pressure drops simulation. (b): Schematic variation of center-line pressure in duct with bend with identification of various pressure drop components [1].

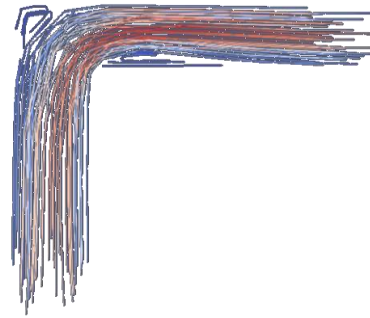
### 5.1 Effect of Reynolds number

Streamlines plots of the velocity in the symmetry plane ( $z = 0$ ) for a sharp  $90^\circ$  bend at different  $Re$  numbers are presented in Figure 7. There is no flow separation for the flow with  $Re < 50$ , which is dominated by viscous forces. Separation at the inner corner appears at  $Re$  of 100, while significant recirculation at the outer corner appears at  $Re$  equal to 200. For  $Re$  equal to 1000 and above, the shape and size of the inner recirculation bubble become almost constant.

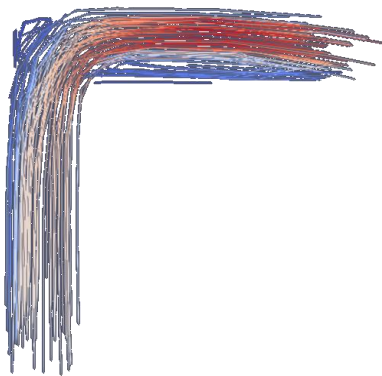
(a)



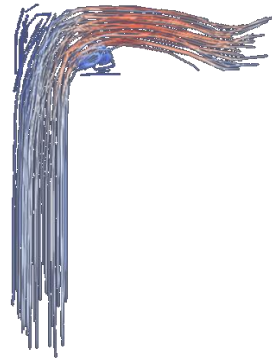
Re = 50



Re = 210

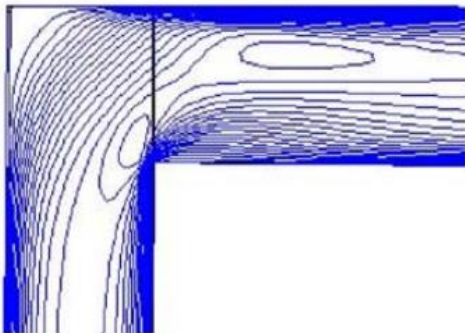


Re = 700

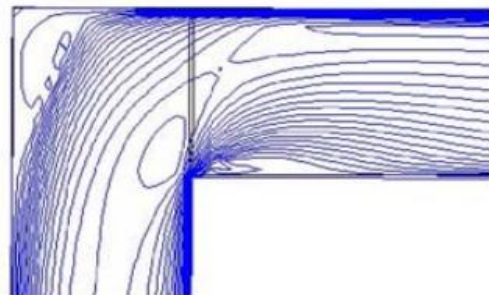


Re = 1900

(b)



Re = 50



Re = 210

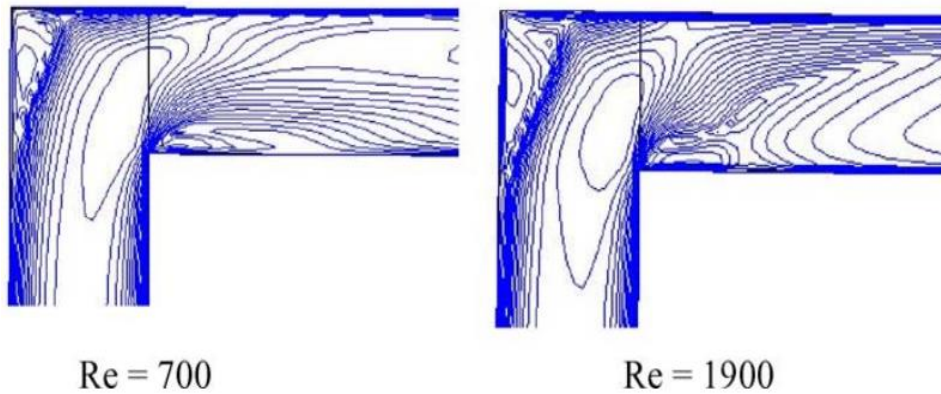


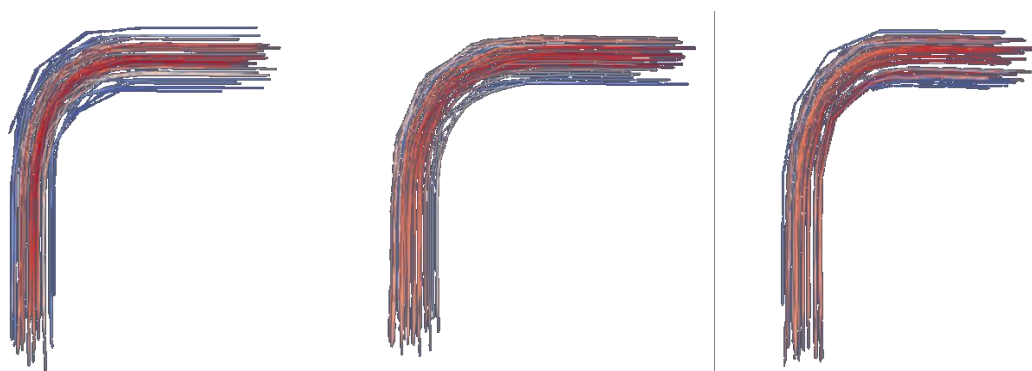
Figure 7. (a): Velocity streamlines plots at various Reynolds for sharp bend ( $A = 2.77$ ) at different Reynolds numbers near the bend. (b): Velocity contour plots at various Reynolds for sharp bend ( $A = 2.77$ ) at different Reynolds numbers near the bend [1].

## 5.2 Effect of curvature ratio

For a gradual bend, i.e., for non-zero values of  $Re$ , no recirculation patterns are observed in the symmetry plane ( $z = 0$ ) for all the  $Re$  and  $Rc/Dh$  ratios investigated. On the other hand, recirculation is observed at the outer wall near the  $z$  planes away from the symmetry plane at high  $Re$ . This is illustrated in Figure 8(i) where the velocity represented by streamlines in the plane close to the bottom wall are compared for different curvature ratios at the same Reynolds number.

There are no recirculation zones throughout the bend as well as in the upstream and downstream sections. Some distortion in the flow near the outer wall of the bend can be observed at  $Re$  greater than 1500. Similar results are obtained for a curvature ratio of 5.66. These results were obtained for an aspect ratio of 2.77.

(i)



$C = 1.41$

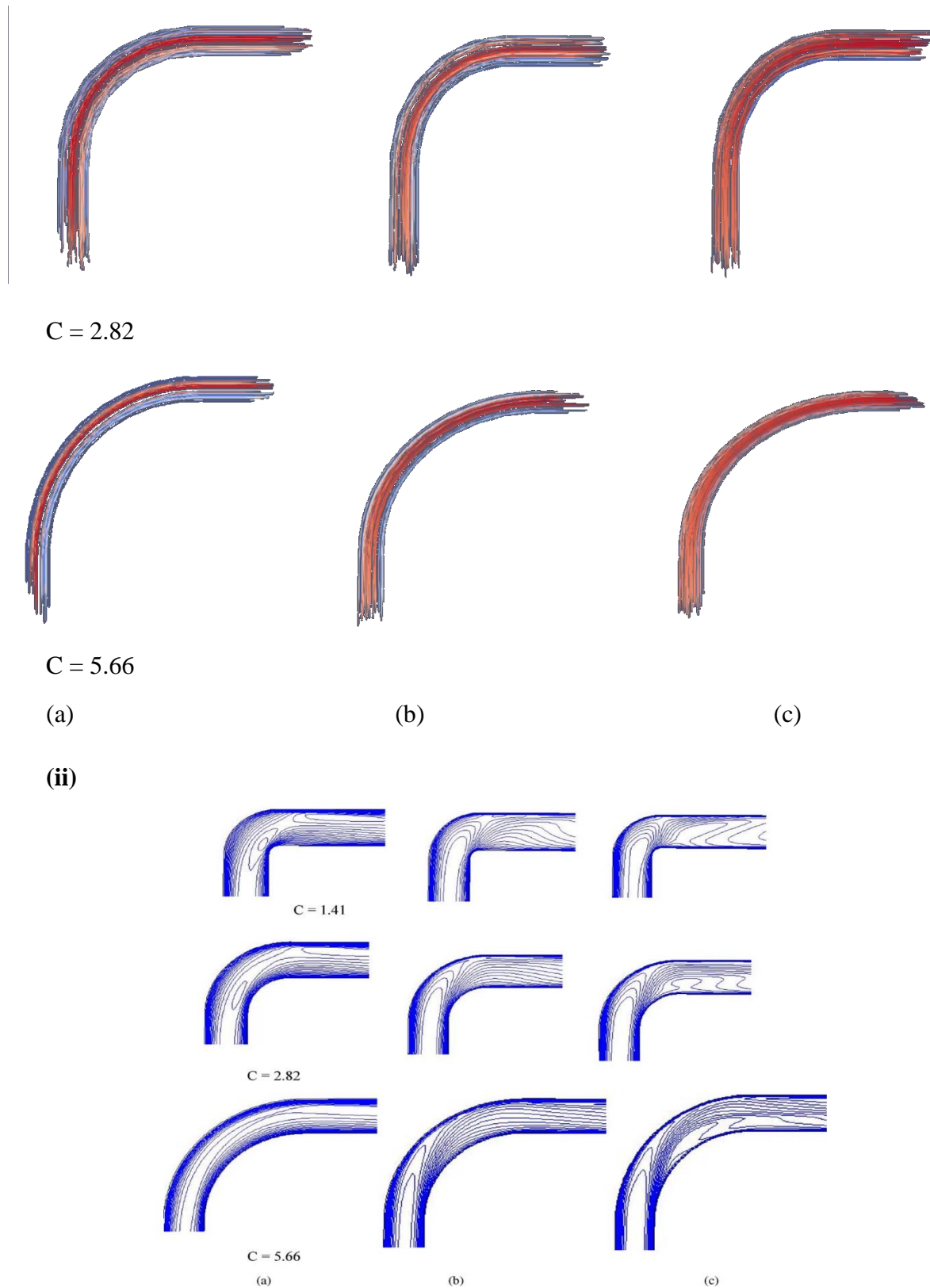


Figure 8.(i): Velocity streamlines plots for different curvature ratios (C) at Reynolds numbers: (a) 100 (b) 700 and (c) 2100 near the wall plane. (ii): Velocity contour plots for different curvature ratios (C) at Reynolds numbers: (a) 100 (b) 700 and (c) 2100 near the wall plane [1].

### 5.3 Effect of aspect ratio

The variation of aspect ratios studied in the experiment reported by [1] to see the velocity contour plots for different spacer lengths ( $6 \cdot Dh$ ) and ( $2 \cdot Dh$ ) at Reynolds number of 700 in symmetry plane of  $180^\circ$  bends. But in this case (as additional work), simulations were done for the geometries of aspect ratios  $A=13.3$ , and  $A=1.36$  in two different Re numbers. The result shows that as the aspect ratio increases, the extent of flow distortion within the bend decreases. When the Re number increases, the recirculation bubbles increase, which is illustrated in Figure 9.

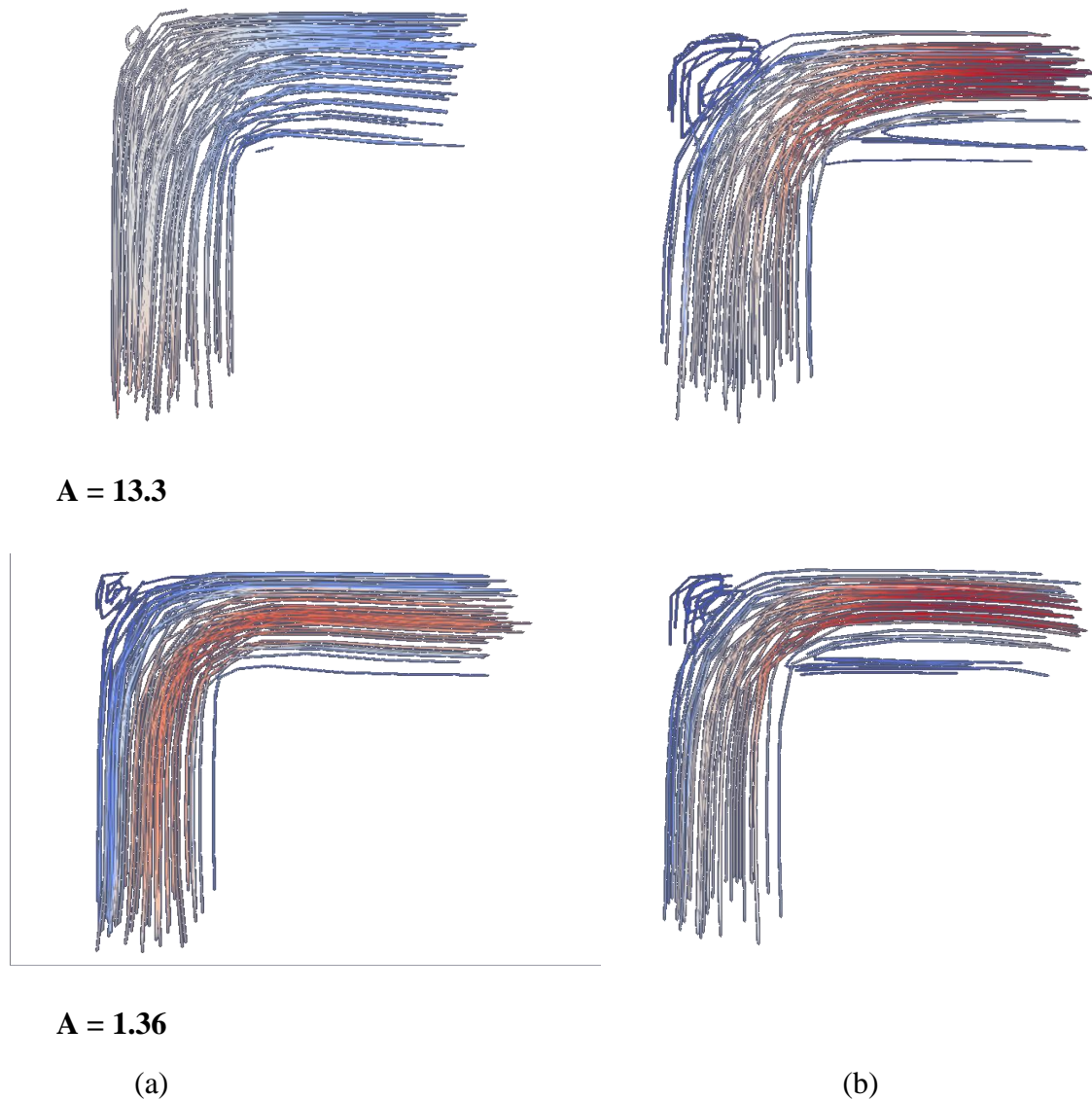


Figure 9: Velocity streamlines plots for different aspect ratios (C) at Reynolds numbers: (a) 50 and (b) 700.

## 5.4 Effect of the fuel temperature

The simulation was done for heat transfer from the fuel flowing (as additional work), assuming the air flowing with a temperature is 433 kelvin and boundary temperature at room temperature which is considered 300 kelvin. buoyantSimpleFoam solver was used, considering some parameters as follows:

- A Specific heat capacity of air is 1004.4 J/kg K.
- Dynamic viscosity of air is  $2.1 \times 10^{-5}$  Pa.s at 433 K.
- Molecular weight of air is 28.96 g/mole.
- Prandtl number of air is 0.705.
- Air is treated as a perfect gas.

The results show that the temperatures are constant and this is the first assumption in the reference paper [1]. This is illustrated in Figure 10.



Figure 10: A sharp bend's temperature distribution along the symmetry plane.

## 6 Conclusion

The simulations have been conducted for 90° bends with different curvature ratios and different aspect ratios. The simulations show that there is a significant effect of Re on the bend loss, which is also influenced by the curvature ratios as well as the presence of the aspect ratios. The more pressure drop happens within the bend cause of wall friction and bends losses, and within the down/upstream there is only wall friction

When increasing the number of cells in the grid independence test from 5376 to 21504 cells, the results do not change significantly, almost constant, therefore taking into consideration the accuracy and computational cost, the number of cells as 5376 is considered for a simulation.

**References**

[1] S. Jayanti, S. Maharudrayya, A.P. Deshpande, “Pressure losses in laminar flow through serpentine channels in fuel cell stacks”, Department of Chemical Engineering, IIT Madras, India, June 2004.

[2] Prasun Dutta, Sumit Kumar Saha, Nityananda Nandi, Nairit Pal, “Numerical study on flow separation in 90° pipe bend under high Reynolds number by k-ε modeling” , Department of Aerospace Engineering and Applied Mechanics, Indian Institute of Engineering Science and Technology, Shibpur, Howrah 711103, India, 2016.

[3] [https://www.engineeringtoolbox.com/air-absolute-kinematic-viscosity-d\\_601.html](https://www.engineeringtoolbox.com/air-absolute-kinematic-viscosity-d_601.html)

[4] R. Atan and W.A. Najmi W.M, “Temperature profiles of an air-cooled PEM fuel cell stack under active and passive cooling operation”, 2012.

DISCLAIMER: This project reproduces the results from an existing work, which has been acknowledged in the report. Any query related to the original work should not be directed to the contributor of this project.